Supporting Information

Coupling of High Ion Transport Efficiency in Hydrogel Electrolytes and Interfacial Fusion for Performance Enhancement in All-Solid-State Paper-Based Self-Powered Electrochromic Devices with Low-Temperature Tolerance

Guodong Liu[a, b, *], Shuyue Chen[a, b], Xiaohong Jiang[a, b], Zhuoqing Zhang[a, b], Yaoli Wang[a, b], Hanbin Liu[a, b], Zhijian Li[a, b], Patrick Gane[c, d]

[a] College of Bioresources Chemical and Materials Engineering, National Demonstration Center for Experimental Light Chemistry Engineering Education, Shaanxi University of Science and Technology, Xi'an 710021, China

[b] Key Laboratory of Functional Printing and Transport Packaging of China National Light Industry, Key Laboratory of Paper-based Functional Materials of China National Light Industry, Shaanxi Provincial Key Laboratory of Papermaking Technology and Specialty Paper Development, Shaanxi University of Science and Technology, Xi'an 710021, China

[c] Department of Bioproducts and Biosystems, School of Chemical Engineering, Aalto University, FI-00076 Aalto, Finland

[d] Faculty of Technology and Metallurgy, University of Belgrade, Karnegijeva 4, 11000 Belgrade, Serbia

* Corresponding author. E-mail: liuguodong@sust.edu.cn

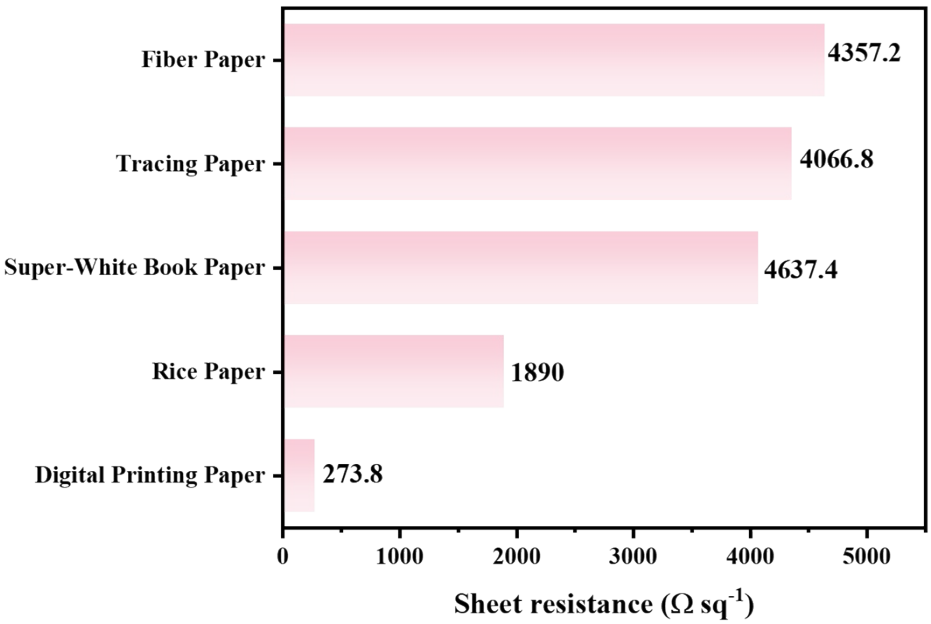

Figure S1. Square resistance of different gravure-printed paper-based electrodes.

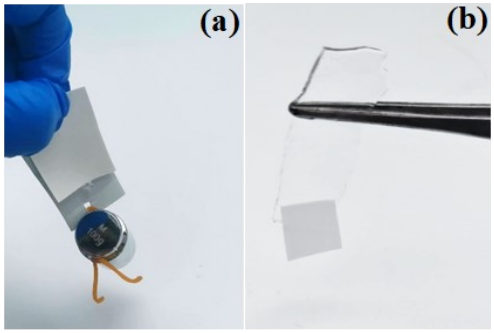

Figure S2. Optical images illustrating the adhesion between the HE and the paper electrodes: (a) two paper electrodes in contact with the HE, with adhesion supporting a 100 g weight, (b) physical demonstration of the HE adhered to a paper electrode.

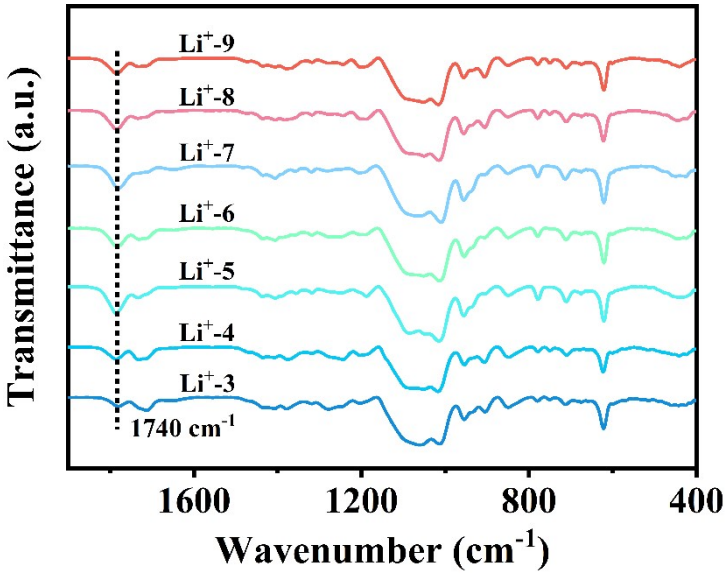

Figure S3. FT-IR spectra of HEs with different ionic concentrations at 400-1800 cm^{-1}.

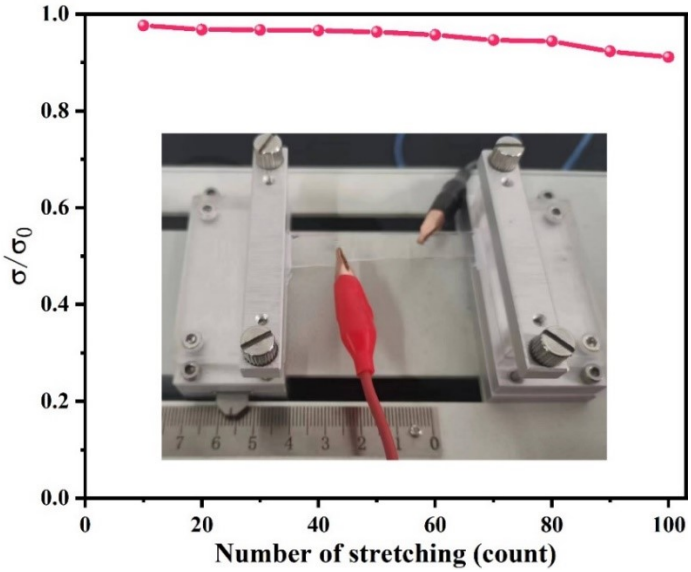

Figure S4. Cyclic tensile curve of the HE.

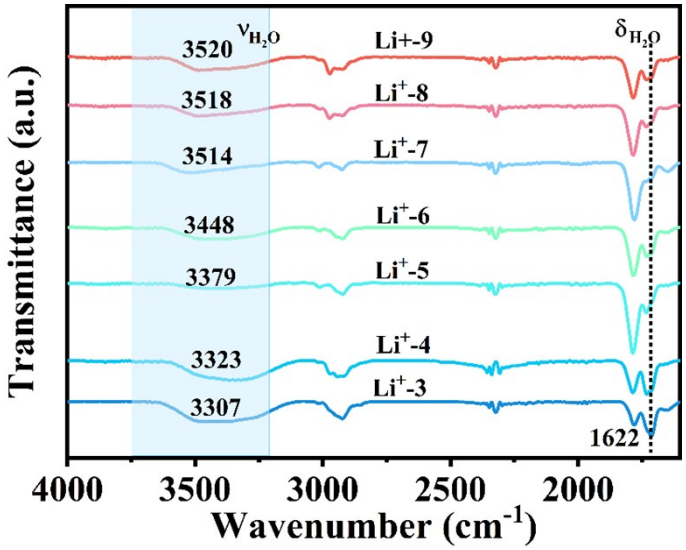

Figure S5. FT-IR spectra of HEs with different ionic concentrations at 1600-2000 cm^{-1}.

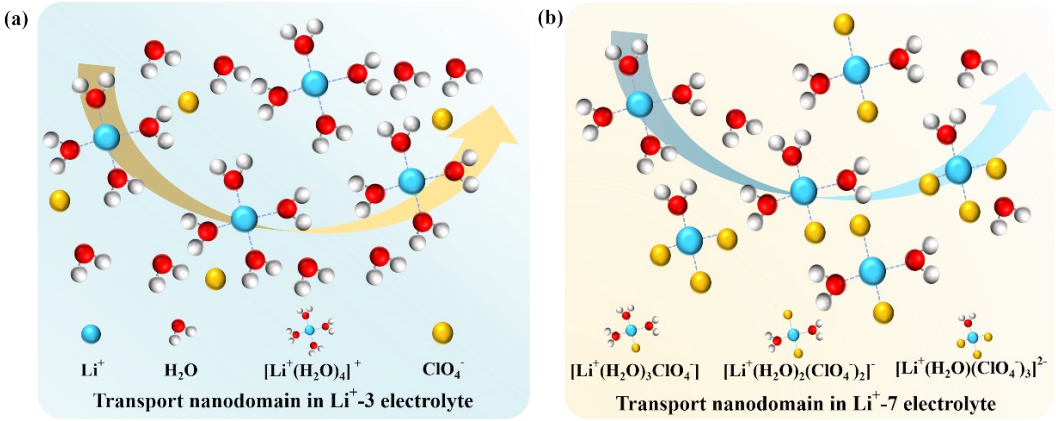

Figure S6. Schematic representation of lithium hydrate ion transport channels in Li^+-3 and Li^+-7 HEs.

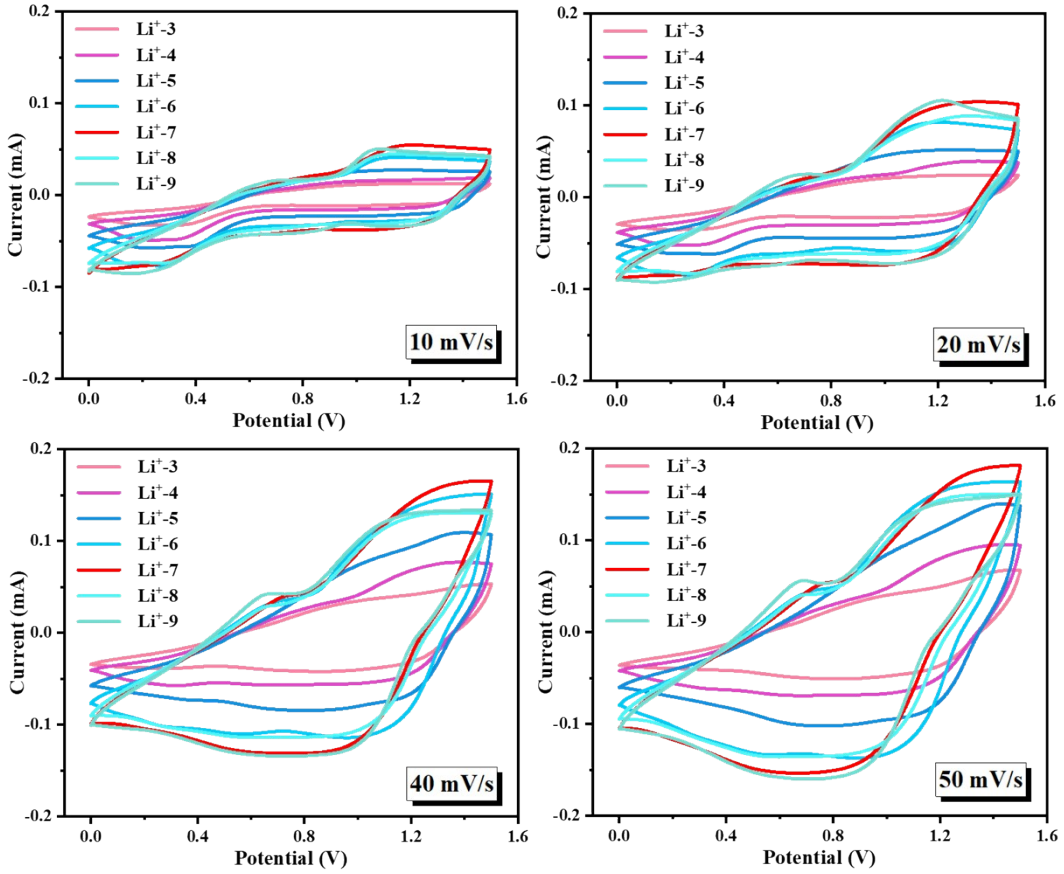

Figure S7. CV curves of self-powered ECDs at different ion concentrations under different scan rates.

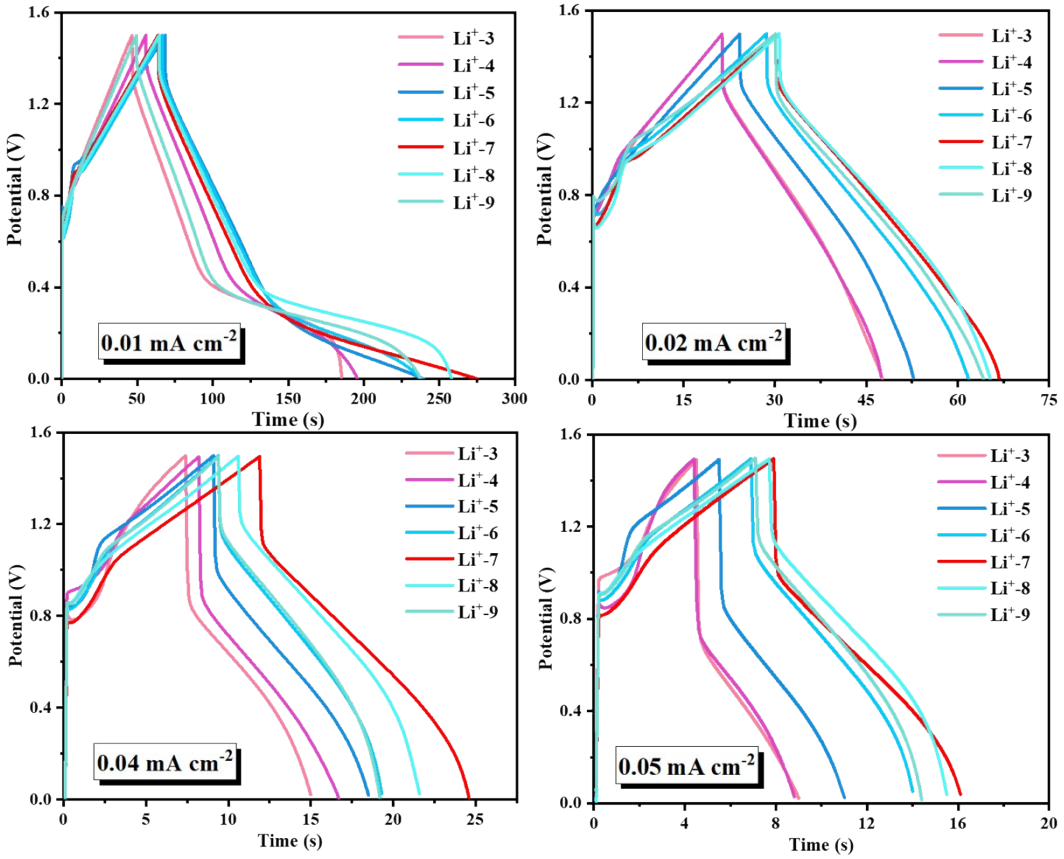

Figure S8. GCD curves of self-powered ECDs at different ion concentrations under different current densities.

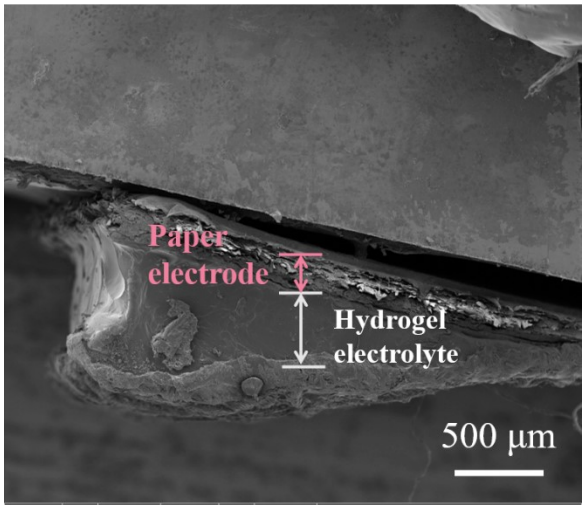

Figure S9. Cross-sectional SEM image of between the electrode and the electrolyte cross-section.

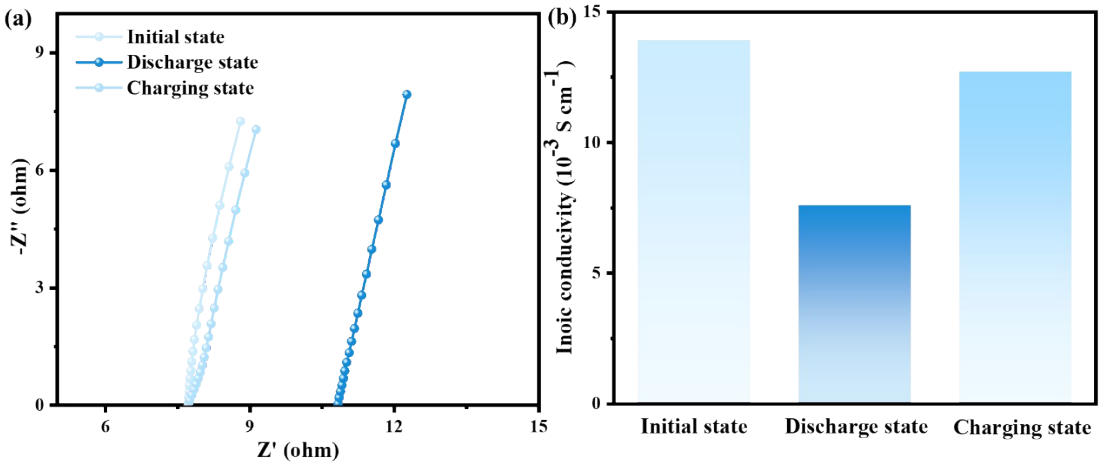

Figure S10. EIS (a) and ionic conductivity (b) of HEs in different states of ECDs.

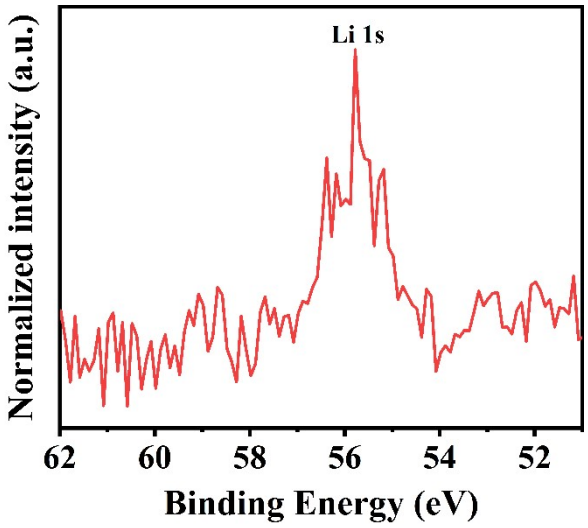

Figure S11. Li 1s XPS spectrum of the PEDOT:PSS electrode.

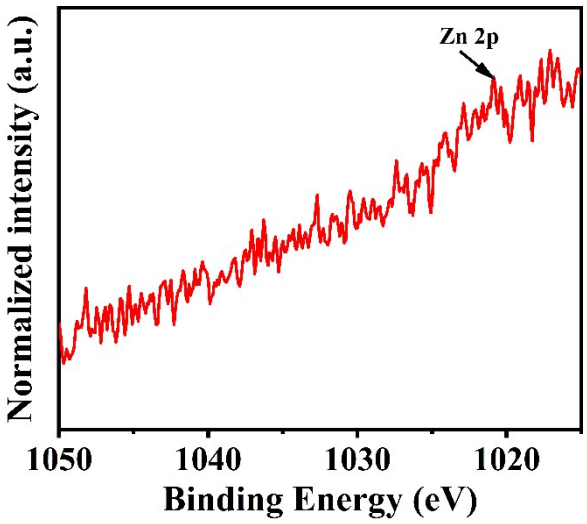

Figure S12. Zn 2p XPS spectrum of the PEDOT:PSS electrode.

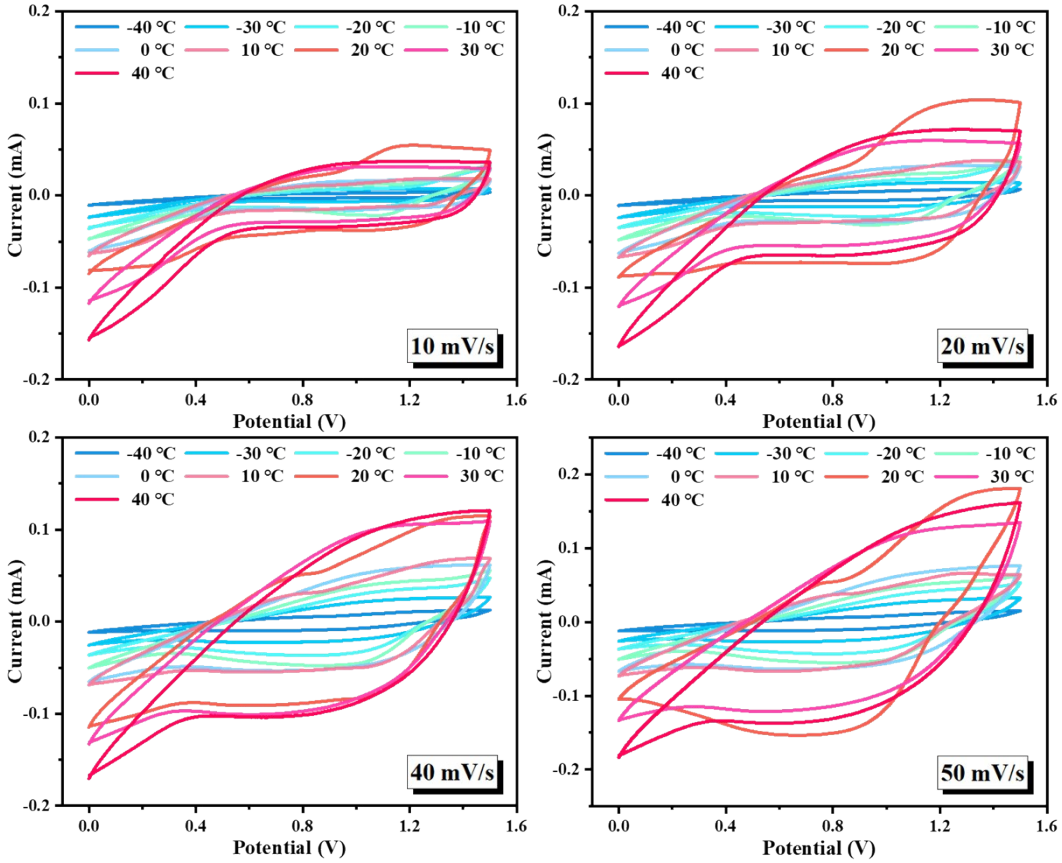

Figure S13. CV curves of self-powered ECD based on Li^+-7 HE at different temperatures under various scan rates.

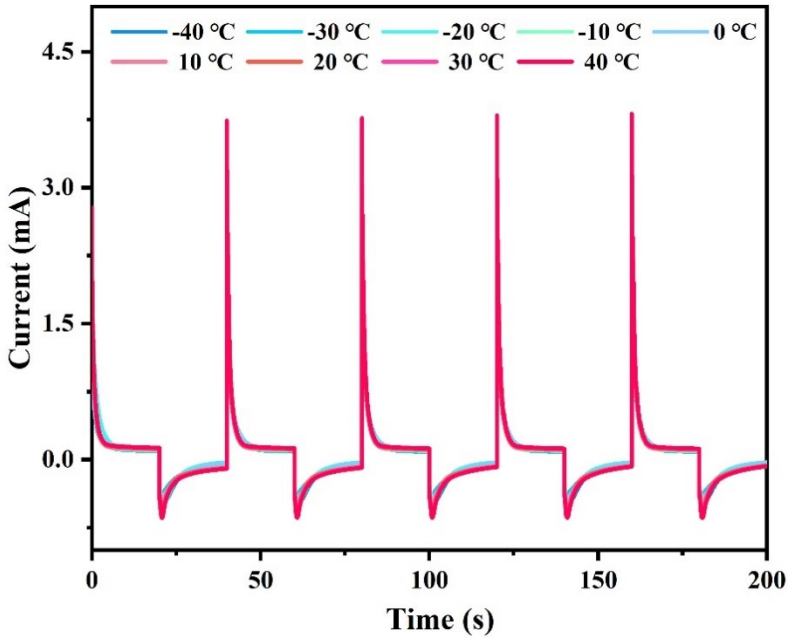

Figure S14. CA curves of the self-powered ECD based on Li^+-7 HE.

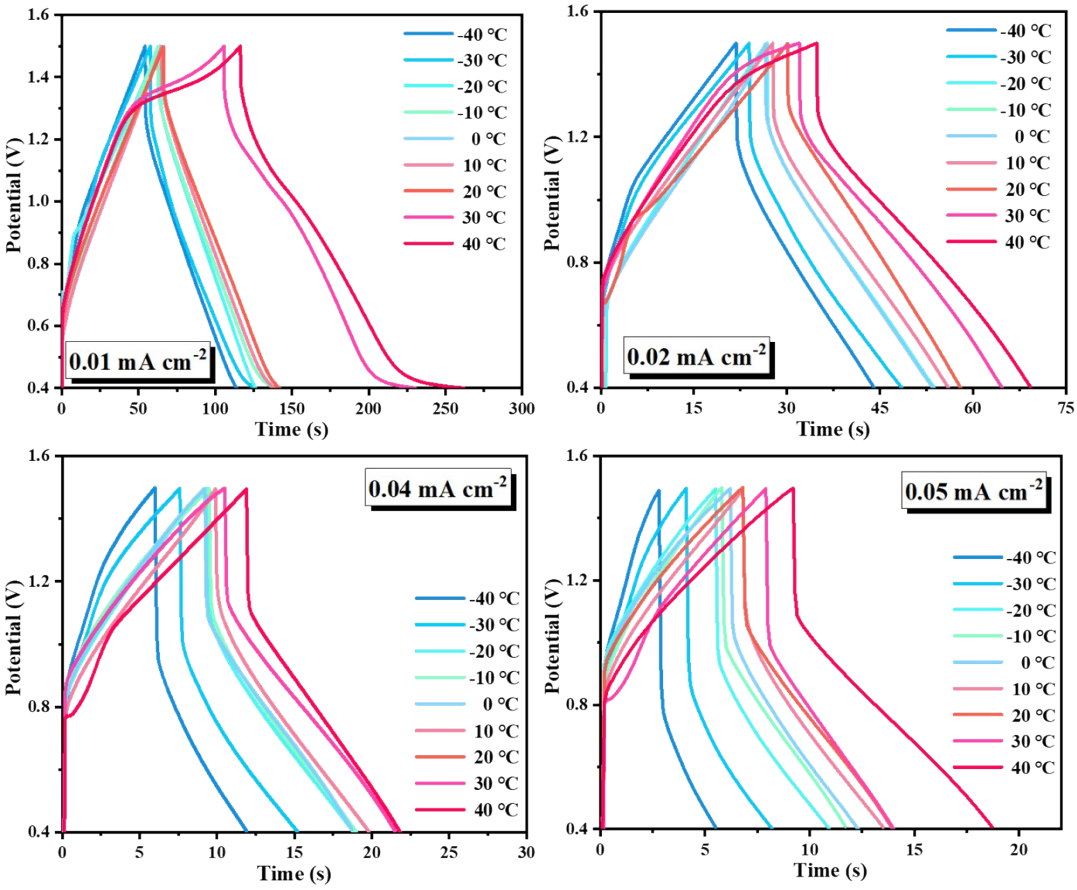

Figure S15. GCD curves of the self-powered ECD based on Li^+-7 HE.